Off-axis electron holography of exchange-biased CoFe/FeMn patterned nanostructures

R. E. Dunin-Borkowski[a] and M. R. McCartney
Center for Solid State Science, Arizona State University, Tempe, Arizona 85287-1704

B. Kardynal[b]
Center for Solid State Electronics Research, Arizona State University, Tempe, Arizona 85287-6206

M. R. Scheinfein
Department of Physics and Astronomy, Arizona State University, Tempe, Arizona 85287-1504

David J. Smith
Department of Physics and Astronomy and Center for Solid State Science, Arizona State University, Tempe, Arizona 85287

S. S. P. Parkin
IBM Almaden Research Center, 650 Harry Road, San Jose, California 95120

(Received 9 April 2001; accepted for publication 8 June 2001)

Off-axis electron holography and micromagnetic simulations have been used to investigate magnetization reversal mechanisms and remanent states in exchange-biased submicron $Co_{84}Fe_{16}/Fe_{54}Mn_{46}$ patterned elements. Domain structures within the elements were characterized despite the narrow thickness (~3 nm) of the ferromagnetic layer relative to the total element thickness (~42 nm). Individual elements were able to support different remanent states and their magnetic microstructure was sensitive to their size. The simulations confirmed that the coercivities of the elements and their domain structures were highly sensitive to the strength and orientation of the pinning field. A good fit to the experimental data was provided by using an interface exchange field that had a fixed amplitude and direction in the simulations, and small disagreements were attributed to structural imperfections. These differences emphasize the value of an experimental technique such as electron holography for probing local micromagnetic structure in individual nanostructured elements. © *2001 American Institute of Physics.* [DOI: 10.1063/1.1390493]

I. INTRODUCTION

Spin-valve (SV) and magnetic tunnel junction structures, which consist of two ferromagnetic (FM) layers separated by a thin metallic or insulating spacer layer, respectively, are of current interest due to the sensitivity of their resistance to the direction and strength of an external magnetic field.[1,2] It is common practice to pin, or ''exchange bias,'' the magnetization direction of one of the FM layers by using an adjacent antiferromagnetic (AF) material such as FeMn,[3] thereby maximizing the change in resistance when the magnetization direction of one of the layers is switched from being parallel to the second layer to antiparallel. Electron microscopy has been used to characterize the microstructure of exchange-biased SVs.[4–7] Lorentz electron microscopy, which is sensitive to magnetic microstructure, has also been applied to investigate magnetization reversal mechanisms in SV structures.[8–11]

With the recent trend toward reduced device dimensions, there is an increasing need for quantitative micromagnetic information about individual nanostructured magnetic elements. Imaging techniques such as electron holography can be used to characterize magnetic features within nanostructures on a nm scale. We have previously used this technique to investigate magnetic interactions in patterned Co nanostructures[12,13] and Co/Au/Ni trilayers.[14] In this article, we describe an electron holography study of patterned submicron elements that contain thin CoFe layers exchange biased by FeMn. We also compare our experimental results with micromagnetic simulations based on the Landau–Lifshitz–Gilbert (LLG) equations.[15]

II. EXPERIMENTAL DETAILS

Exchange-biased elements were patterned using standard electron-beam lithography and lift-off processes.[12] The elements consisted of [Ti (5 nm)/Pd (15 nm)/$Fe_{54}Mn_{46}$ (10 nm)/$Co_{84}Fe_{16}$ (2.8 nm)/Al_2O_3 (2 nm)/Pd (7.5 nm)], as illustrated schematically in Fig. 1(a). A thin Ti seed layer was included to enhance the ⟨111⟩ texture of the films. The elements were prepared by sputter deposition directly onto self-supporting 55-nm-thick silicon–nitride membranes, and the exchange field of the AF was set using a 120 Oe horizontal field during deposition. Because of the sample geometry, the direction of this field was rotated by 15° from the line joining adjacent elements.

[a]Author to whom correspondence should be addressed. Present address: Department of Materials Science and Metallurgy, Pembroke Street, Cambridge CB2 3QZ, UK; electronic mail: rafal.db@msm.cam.ac.uk
[b]Present address: Toshiba Research Europe Ltd., Cambridge Research Laboratory, 260 Science Park, Milton Road, Cambridge CB4 4WE, UK.

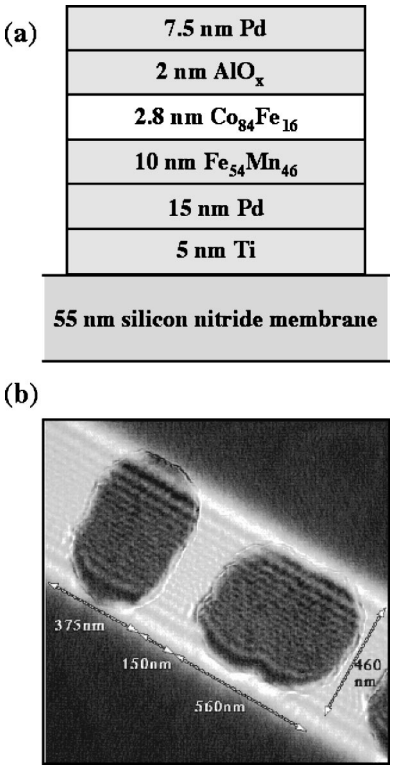

FIG. 1. (a) Schematic diagram showing nominal layer thicknesses in exchange-biased patterned elements; (b) Off-axis electron hologram of two rectangular elements showing typical lateral dimensions.

A Philips CM200ST-FEG transmission electron microscope, equipped with a field-emission electron source and operated at 200 keV, was used for off-axis electron holography.[16] An electrostatic biprism and an additional (Lorentz) minilens were used to record holograms at magnifications of up to ~70 kx and point resolutions of ~2 nm with the normal objective lens of the microscope switched off and the sample located in almost field-free conditions. Magnetization reversal processes could also be followed *in situ* by increasing the objective lens current slightly and tilting the specimen in a known vertical magnetic field, which had been calibrated previously.[11] The representative electron hologram in Fig. 1(b) shows the lateral dimensions of the exchange-biased nanostructures analyzed in this study. The rough particle edges result from the difficulty of performing lift off after the heat treatments used during sample preparation.

Calculations of the magnetization within the exchange-biased elements were performed by solving the LLG equations in the continuum micromagnetic limit. In the absence of measured values for $Co_{84}Fe_{16}$, the polycrystalline film was modeled using bulk Co properties with an exchange stiffness A of 1.55 μerg/cm and a saturation magnetization M_s of 1414 emu/cm^3. The magnetocrystalline anisotropy constant K in the polycrystalline layer (which had a grain size of below 10 nm) was set to zero. A gyromagnetic frequency γ of 17.6 MHz/Oe, and a damping constant α of 1 were used in the LLG calculations, and the effects of temperature fluctuations were not included. Slightly different values for the gyromagnetic frequency have been reported elsewhere,[17] but this will not have any effect on the final equilibrium structure. In-plane, discrete moments, representing a continuous magnetization distribution, were 5.0 nm on each side. A single layer of moments was used for the magnetically active layer, and the demagnetization field was computed to all orders, coupling the moments in all cells with each other.

III. RESULTS AND DISCUSSION

A comparison of (a) holographic phase measurements and (b) micromagnetic simulations around an entire magnetization reversal cycle, proceeding in a counterclockwise direction, is shown in Fig. 2. In these experiments, the component of the applied field in the plane of the sample was varied between ±1930 Oe in an out-of-plane field of ~3600 Oe. (Extreme ends of the loop are not shown.). The in-plane component of the applied field, which is directed along the horizontal axis, is shown at the bottom left corner of each experimental image. [In Fig. 2(a), the contribution of the ''mean inner potential'' to the holographic phase has already been subtracted from each hologram so that the remaining magnetic contribution can be identified.[18]] The direction of the in-plane component of the magnetic induction, integrated in the incident beam direction, is represented using a continuous color wheel (red = right; yellow = down; green = left; blue = up). The intensity of the color represents the magnitude of the induction, as does the density of the phase contours.

The experimental phase contours in Fig. 2(a) reveal several interesting features. No solenoidal or vortex states are visible for either element, and there is significant continuity of the phase contours between the particles over large parts of the loop. For the smaller element (at left), changes in the applied in-plane field result in rotation of the contours, first in a counterclockwise and then in a clockwise sense. Complete reversal is not achieved, perhaps indicating that shape anisotropy has a controlling influence on its behavior. The larger element reverses between 0 and −168 Oe in both directions, which is consistent with the hysteresis offset that may be anticipated for a pinned magnetic layer. Finally, our study of remanent states, as described below, suggests that a vortex state may normally be expected to occur between these two field values.

Simulations showed that the magnetic response was highly nonlinear and hysteretic. The coercivity and the magnetic switching mode depended on the magnetic parameters describing the system as well as on the initial magnetic state and the direction of the applied magnetic field. Although the center of the loop is given by the exchange bias, experimental factors such as strain and local roughness, which are difficult to simulate, affect the strength of the coercive field in practice. For ease of simulation and interpretation, the effect of coupling to the AF was simulated as an interface exchange field with a fixed amplitude of 75 Oe along the line joining the bits and with a variable strength in the perpendicular direction. Position-dependent parameters were used for some simulations but these were discontinued because of issues relating to inversion and uniqueness. As may be

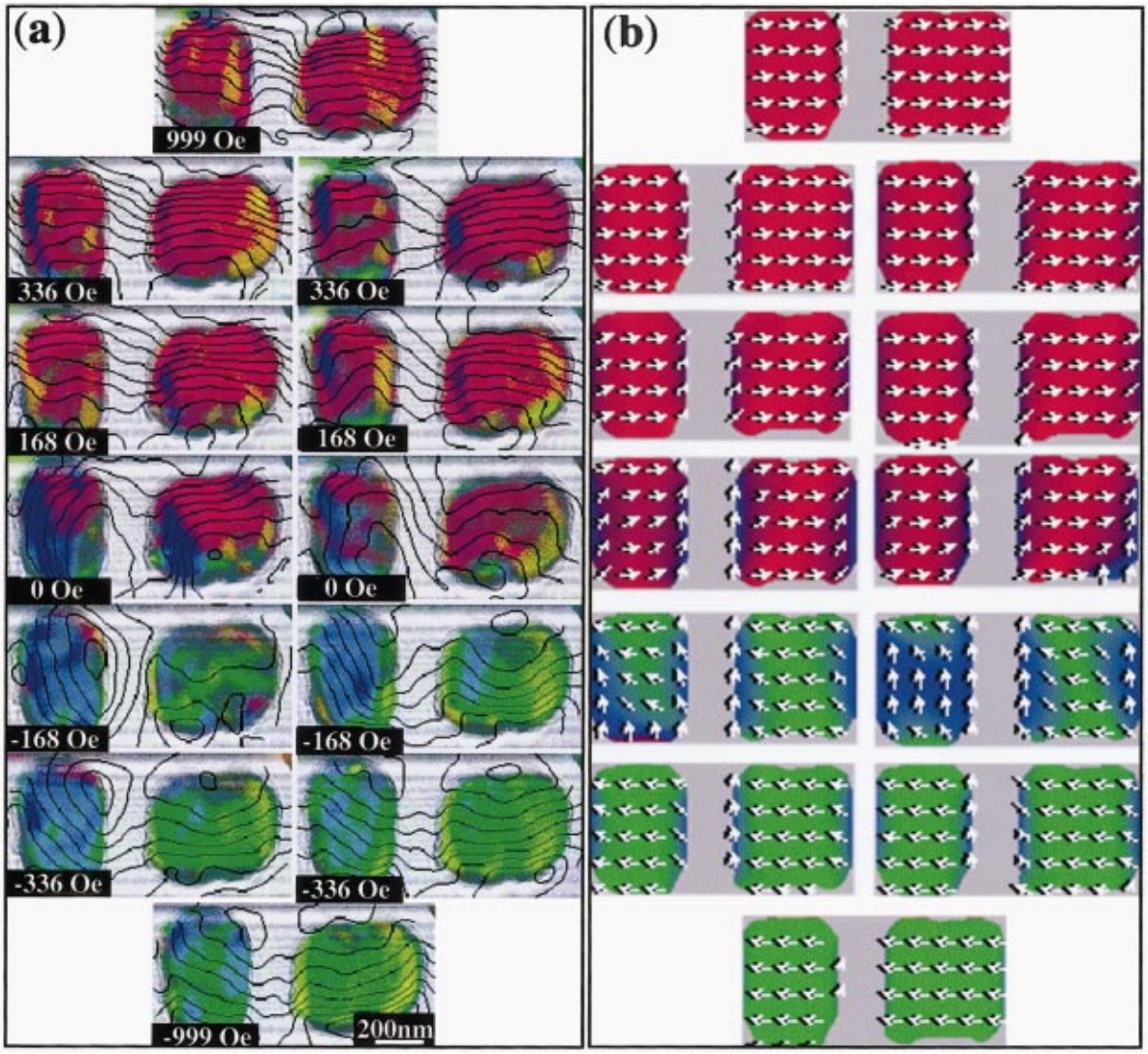

FIG. 2. (Color) Comparison of (a) experimental holographic phase measurements and (b) micromagnetic simulations during complete magnetization reversal cycle for exchange-biased $Co_{84}Fe_{16}/Fe_{54}Mn_{46}$ patterned elements. Applied in-plane fields, which are directed along the horizontal axis, are shown at the bottom left corner of each phase image. Colors represent different magnetization directions. Phase contours are separated by 0.085π radians.

anticipated,[19,20] the effect that this exchange field and its orientation has on the switching mechanism and the coercive field is pronounced. For the best-fitting simulations shown in Fig. 2(b), the exchange field was set to 79 Oe with a counterclockwise rotation of 18° from the line joining the elements. This angle is remarkably close to the 15° angle used during deposition, particularly considering the possibility that the sample may not be precisely flat during the experiments.

Figure 3 compares experimental and simulated hysteresis loops for the larger of the two elements. In Fig. 3(a), which was measured from the experimental holograms, the loop is shifted sideways from zero by about 90 Oe due to the influence of the pinning layer. This value for the exchange field is at the lower end of the range reported[20] for FeMn exchange-biased SVs that are in the form of continuous thin films, rather than the patterned elements observed here. The simulated loop shown in Fig. 3(b) shows the fractional magnetization M/M_s in the direction of the applied field plotted for the configuration that provided the best agreement with the experimental data. The experimental loop is broader than the simulated loop, suggesting the presence of nonuniform coupling, perhaps due to the finite grain size affecting roughness.

Figure 4 shows a selection of remanent states measured for the two elements. Before recording each image, a large

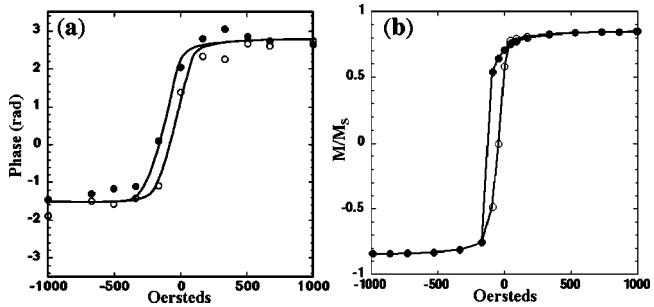

FIG. 3. Hysteresis loops for larger exchange-biased element: (a) measured from experimental holograms; (b) derived from micromagnetic simulations.

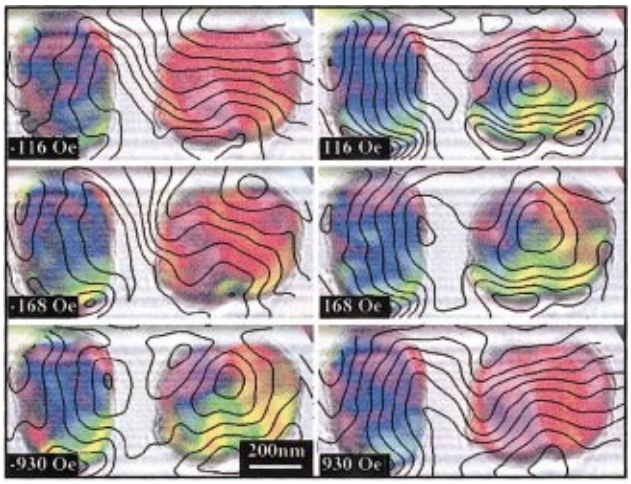

FIG. 4. (Color) Remanent states for exchange-biased elements. Left-hand set obtained after saturation of elements to the right followed by reversal to the value indicated. Similarly for the right-hand set except initial saturation direction to the left.

positive (or negative) in-plane field was applied to the sample to ensure complete magnetization. Then a field of the value indicated was applied in the opposite direction. Finally, the field was reduced to zero and the corresponding electron hologram was recorded. The difference in behavior between the two elements is striking. Whenever the larger (*RH*) element is magnetized to the right, as defined by the hysteresis loop in Fig. 3(a), the remanent state is a single domain pointing to the right. Conversely, whenever it is magnetized to the left, the remanent state is a single vortex. The smaller (*LH*) element behaves differently, again suggesting that its behavior is influenced by shape anisotropy. Its remanent state is invariably a single domain pointing in the upward direction. It is perplexing that the spacing of the contours in this element, when the initial magnetizing field is applied to the right, is about half the spacing observed when the field is initially applied to the left. [Similar behavior is observed in the larger element at −168 Oe in Fig. 2(a)]. This result suggests that the magnetization of the FM layer may have an out-of-plane component that is not understood at present.

In a previous study of Co nanostructures,[13] switching asymmetry was caused by the out-of-plane component of the applied field, and strong intercell coupling also occurred. Both effects are again likely to be present, in addition to the effect of the pinning field. The results described here will depend on the specific dimensions and thicknesses of these exchange-biased elements, as demonstrated in previous theoretical[19,20] and experimental[21,22] studies, and it would be of particular interest to compare sheet films and patterned elements.[23] Nevertheless, it is apparent that extrapolation from bulk macroscopic behavior is inadequate for predicting micromagnetic response. Indeed, discrepancies between the electron holography results and micromagnetic simulations emphasize that local structural irregularities are likely to play an increasingly important role as device dimensions continue to shrink.[14,24] Further systematic studies are now required to pinpoint the role of exchange anisotropy in such structures.

ACKNOWLEDGMENTS

This work was partly supported by an IBM subcontract on the DARPA Advanced MRAM Project under Contract No. MDA-972-96-C-0014. The authors thank James Speidell for providing Si_3N_4 membranes and they acknowledge the use of facilities in the Center for High Resolution Electron Microscopy at Arizona State University. R.E.D. thanks the Royal Society for financial support.

[1] B. Dieny, V. S. Speriosu, S. S. P. Parkin, B. A. Gurney, D. R. Wilhoit, and D. Mauri, Phys. Rev. B **43**, 1297 (1991).
[2] S. S. P. Parkin, Annu. Rev. Mater. Sci. **25**, 357 (1995).
[3] J. C. S. Kools, IEEE Trans. Magn. **32**, 3165 (1996).
[4] L. Tang, D. E. Laughlin, and S. Gangopadhyay, J. Appl. Phys. **81**, 4906 (1997).
[5] K. M. Krishnan, C. Nelson, C. J. Echer, R. F. C. Farrow, R. F. Marks, and A. J. Kellock, J. Appl. Phys. **83**, 6810 (1998).
[6] X. Portier, A. K. Petford-Long, P. Gayle-Guillemaud, T. C. Anthony, and J. S. Brug, Appl. Phys. Lett. **72**, 118 (1998).
[7] B. Y. Wong, C. Mitsumata, S. Prakash, D. E. Laughlin, and T. Kobayashi, J. Appl. Phys. **79**, 7896 (1996).
[8] M. F. Gillies, J. N. Chapman, and J. C. S. Kools, J. Appl. Phys. **78**, 5554 (1995).
[9] T. G. S. M. Rijks, R. F. O. Reneerkens, R. Coehoom, J. C. S. Kools, M. F. Gillies, J. N. Chapman, and W. J. M. de Jonge, J. Appl. Phys. **82**, 3442 (1997).
[10] X. Portier, A. K. Petford-Long, T. C. Anthony, and J. A. Brug, Appl. Phys. Lett. **75**, 1290 (1999).
[11] A. K. Petford-Long, X. Portier, P. Bayle-Guillemaud, T. C. Anthony, and J. A. Brug, Microsc. Microanal. **4**, 325 (1998).
[12] R. F. Dunin-Borkowski, M. R. McCartney, B. Kardynal, and D. J. Smith, J. Appl. Phys. **84**, 374 (1998).
[13] R. E. Dunin-Borkowski, M. R. McCartney, B. Kardynal, D. J. Smith, and M. R. Scheinfein, Appl. Phys. Lett. **75**, 2641 (1999).
[14] D. J. Smith, R. E. Dunin-Borkowski, M. R. McCartney, B. Kardynal, and M. R. Scheinfein, J. Appl. Phys. **87**, 7400 (2000).
[15] M. R. Scheinfein, J. Unguris, J. L. Blue, K. J. Coakley, D. T. Pierce, R. J. Celotta, and P. J. Ryan, Phys. Rev. B **43**, 3395 (1991).
[16] M. R. McCartney, D. J. Smith, R. F. C. Farrow, and R. F. Marks, J. Appl. Phys. **82**, 2461 (1997).
[17] M. Mansuripur, *Physical Principles of Magneto-Optical Recording* (Cambridge University Press, Cambridge, 1995), p. 567.
[18] R. E. Dunin-Borkowski, M. R. McCartney, D. J. Smith, and S. S. P. Parkin, Ultramicroscopy **74**, 61 (1998).
[19] T. Ambrose, R. L. Sommer, and C. L. Chien, Phys. Rev. B **56**, 83 (1997).
[20] H. Xi and R. M. White, J. Appl. Phys. **86**, 5169 (1999).
[21] P. Bayle-Guillemaud, A. K. Petford-Long, T. C. Anthony, and J. A. Brug, IEEE Trans. Magn. **32**, 4627 (1996).
[22] R. Jungblut, R. Coehoorn, M. T. Johnson, J. de Stogge, and A. Reinders, J. Appl. Phys. **75**, 6659 (1994).
[23] J. G. Zhu, Y. Zheng, and X. Liu, J. Appl. Phys. **81**, 4336 (1997).
[24] J. Gadbois, J.-G. Zhu, W. Vavra, and A. Hurst, IEEE Trans. Magn. **34**, 1066 (1998).